Modeling a Circulating Fluidized Bed $CaCO_3$ calcination reactor for Thermochemical Energy Storage in a Concentrating Solar Power system

Mayra Alvarez Rivero
mayra.alvarez.rivero@gmail.com
Department of Energy Engineering and Management
Instituto Superior Técnico, Universidade de Lisboa, Portugal

Abstract

A new unidimensional, steady-state computational model was developed to simulate a calciner for the application of calcium looping as a way of thermochemical energy storage in concentrating solar power systems. The proposed reactor is an absorber tube enclosed within a reflective cylindrical cavity. The absorber tube is also the riser of a circulating fluidized bed where the calcination reaction proceeds. The proposed model heat transfer processes are based on the core-annulus model and the hydrodynamic proposed model is a modified version of the K-L model. The model considers the change in the mass flow rate of species and the density change of the phases in the axial direction of the reactor, which is usually considered constant in the available models from the literature. It was verified that assuming a constant density and a constant mass flow rate, leads to an efficiency increase up to 5% points for the studied conditions in the reference case. Simulations were performed imposing a constant wall temperature or non-uniform heat flux distribution on the reactor wall. The simulation shows that a 6 m height reactor allows achieving a calcination efficiency of 65 % for the conditions of the reference case. Higher heights do not contribute significantly to the efficiency increase. A sensitivity study shows that the decay factor, the inlet temperature of the bed, the mass fraction of CO_2 at the inlet, and the ratio between the gas and solids mass flow rates are the parameters that affect the most the efficiency of the process.

Keywords: Solar Reactor, Calciner, Circulating Fluidized Bed (CFB), Calcination, 1-D Model, Calcium Looping (CaL).

1. Introduction

Concentrating Solar Power (CSP) is unique among the renewable energy sources because it can easily be coupled with thermal energy storage (TES) making it highly dispatchable. Key categories for TES for CSP system are sensible TES (e.g. molten salts and packed beds), latent heat TES (e.g. encapsulated PCM), and Thermochemical Energy Storage (TCES) (e.g. carbonates, hydroxides, and metal redox) [1]. The major commercial solution used nowadays is molten-salt technologies accounting for 75 % of the globally installed TES capacity. However, molten-salt as Heat Transfer Fluid (HTF) has several disadvantages: its corrosiveness, its maximum working temperature (~560 °C), which limits the system efficiency, and the significant energy consumption required to keep the molten salts at temperatures over 220 °C to avoid solidification [2]. In counterpart, TCES is an option that allows storing energy at higher densities [1]. Several reactions for TCES have been proposed with carbonates, hydroxides, metal redox, sulfur, hydrides, methanol, and ammonia.

One of the most promising systems relies upon the calcination-carbonation reaction of $CaCO_3$-CaO and it is known as Calcium Looping (CaL) process (Fig. 1). In this system, the concentrated solar power is used to carry out the endothermic calcination reaction that releases CaO and CO_2 as products.

$$CaCO_3(s) \Leftrightarrow CaO(s) + CO_2(g),\ \Delta H_{cal} = 178.4 \quad (1)$$

These products are stored separately and when needed, they are brought together to carry out the exothermic carbonation reaction to release the stored energy. The main advantages of a CaL process over molten salts and other TCES systems are: (i) the low cost, wide availability and harmlessness of natural CaO precursors as limestone and dolomite, (ii) the high energy density of the CaL system ($3 - 4$ GJ.m^{-3}) is one of the largest among TCES systems, and (iii) the high reaction turning temperature of carbonation. The application of CaL for TES would overcome the current CSP temperature limitations of 550 to 600 °C for molten salts.

The CaL process has been conceptualized initially for post-combustion CO_2 capture and nowadays there are lab- and pilot-scale plants that have demonstrated the process successfully, e.g. 30 kW at INCAR-CSIC in Spain [3], 10 kW and 200 kW at the University of Stuttgart [4] [5], 1.7 MW at La Pereda in Spain [6], and 1 MW at TU Damstadt in Germany [7].

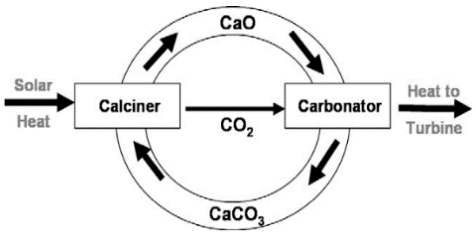

Fig. 1. Calcium looping system applied to solar power thermal transport and storage.

2. Objectives and Methodology

The main goal of this study is to develop a model of a reactor for the calcination of $CaCO_3$ considering that it would be later coupled with a CSP system for TCES. The steps to follow to achieve this includes: (i) to review the state of the art of solar reactors for the thermal decomposition of $CaCO_3$ and other chemical reactions to discuss and ponder the benefits and downsides of different technologies, (ii) to select a reactor concept based on the type of flow in the reactor and the heat integration mode into the reaction chamber, (iii) to establish the geometry, materials and operating conditions of the reactor based in current CaL plants, and (iv) to develop a model that describes the reaction kinetics, hydrodynamics, and heat transfer inside the reactor for the case of constant wall temperature and non-uniform flux distribution. The proposed model would be used to identify the most important parameters affecting the reactor efficiency that would need to be considered when building a prototype of the concept. Table 1

summarizes typical conditions for the CaL process of post-combustion of CO_2 and compares it with those for TCES applications.

Table 1. Typical condition for CaL systems for the post-combustion of CO_2 and TCES [2].

CaL process application	Typical conditions	
	Calcination	Carbonation
Post-combustion CO_2 capture	950 °C (high CO_2 atmosphere) P=1 atm	650 °C 15% v/v CO_2 P=1 atm
Thermochemical Energy Storage	~725 °C/900-950 °C (He or H_2O/CO_2 atmosphere) P=1 atm	~850 °C Pure CO_2 P = 1-5 atm

3. State of the Art of Solar Receivers/Reactors

In the literature, it can be found different types of solar reactors classification depending on different criteria [8], [9]. In this work, two of the categories presented by Zsembinszki et al. [9] are considered, i.e. the heat integration mode into the reaction chamber, which is based on the interaction between solar radiation and the thermochemical reactor, and the flow pattern inside the reactor, which has to do with the presence of a carrier fluid and its contact with the particles (Fig. 2).

In indirectly irradiated reactors, the reactant does not receive direct concentrated irradiance. These reactors rely on a primary absorber where the heat resulting from the concentrated radiation is received and transferred to the reactant or a secondary cavity where the reactant is. In directly irradiated reactors, the reactant is irradiated and heated by the solar radiation avoiding having an intermediary surface. However, in these reactors, there is an aperture that can be open or closed with a quartz window. The design of the window is a challenge. Literature reports complications as degradation, cracking and clogging of the suction system to keep it clear [2], [8]. When considering the flow pattern, solar reactors can be divided into three main groups: stacked bed reactors, fluidized bed reactors, and entrained bed reactors [3]. In fluidized bed reactors, the particles move with the gas flow creating a bubble-induced phenomenon, while in the case of entrained bed reactors, specifically cyclones, the injected gas creates a vortex inside the cavity. In contrast, in stacked bed reactors no gas is injected in the process and the working principle will depend on whether the particles compose a fixed, moving, or rotating bed.

4. Selection of the solar reactor concept

For the selection of the solar reactor concept, forty-nine papers were evaluated. From these, five were review papers, and nineteen were related to limestone calcination. There were some types of configurations that have not been tested for calcination. Therefore, the remaining papers correspond to other available experimental studies dealing with other processes like steam gasification of charcoal and water-splitting for hydrogen production by thermal decomposition of zinc oxide, copper oxide, tin oxide, and cerium oxide.

Two decisions had to be taken when selecting the solar reactor concept to proceed with this work. The first is the heat integration mode into the reaction chamber and the second, the type of flow pattern of the solid-gas flow. From the reviewed papers it was concluded that indirectly heated systems were the preferred concept. The main benefit is the lack of need for a quartz window which could bring complications — namely the risk of degradation

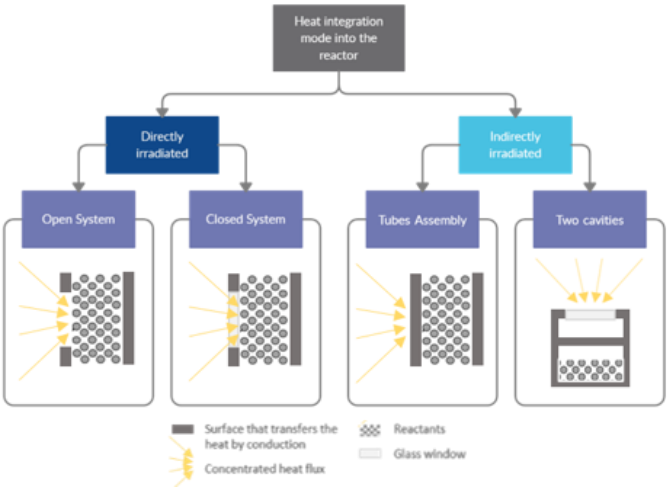

Fig. 2. Solar thermochemical reactors classification based on the heat integration mode into the reaction chamber

and crack of the window, and the clogging of the suction system used to keep it clear. Besides, the use of an intermediate radiating surface helps to smooth the temperature differences reducing the risk of over and under heating the reactant as it passes through different parts of the reactor. The price to pay is on the challenge of distributing the radiation through the irradiated surface, the high temperatures it must stand, and the re-radiation losses through the opening of the cavity. In terms of the flow pattern, it was concluded that the fluidized bed reactor was the preferred option. Its major benefits are its high heat and mass transfer rate, good mixing of solids, adjustable residence time with long permanence in high-temperature zones, and the possibility of continuous operation, i.e. Circulating Fluidized Bed (CFB). From the stacked bed reactors, only rotary kilns showed to perform well under the selected criteria. However, a system with rotating parts adds complexity to the operation of the solar reactor and therefore was discarded. Finally, cyclone reactors were discarded for the short residence time of the particles under the high-temperature zone beside the impossibility of adjusting the residence time of the particles once the reactor is built.

The final concept is an absorber tube, that has the role of the riser of the CFB, inside a reflective cavity with an open aperture (Fig. 3). As an initial step, the objective will be to model and assess the performance of one absorber tube reactor in terms of the reaction kinetics, hydrodynamics, and heat transfer. In future works, this model will be coupled with the reactor's cavity model and the CSP field. With a final tool, it would be possible to test different configurations like several risers inside the reflective cavity.

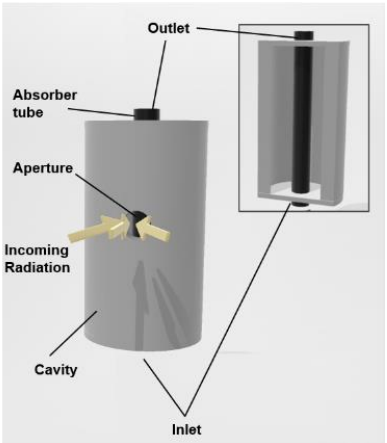

Fig. 3. Isometric view of the proposed reactor with its cross-section. The presented scheme is not to scale.

Table 2. Characteristics reported in reviewed publications for directly and indirectly heated reactors.

Characteristic	Directly Heated Systems		Indirectly Heated Systems
Direct concentrated solar radiation focused on	Reactant		Intermediate radiating surface / sub-surface of the primary cavity
Heating pace	Fast		Slow
Distribution of radiation (among the cavity)	Less challenging		More challenging
Reactors wall temperature	Lower		Higher
Longitudinal thermal gradient across the reaction chamber	High		Low
Hotspots formation	Likely[1]		Unlikely
	Open	Closed	
Gas-tightness and possibility of capturing CO_2 mass	No	Yes	Yes
Risk of cracking of the window	N/A	High	N/A
Risk of degradation of the window for fouling of particles	N/A	High	N/A
Risk of clogging	Low	High	Low
Re-radiation losses through openings	Moderate	Low	Low to high

5. Proposed Mathematical Model

The selection of the operating conditions of the CFB reactor is based on lab-scale CaL plants. Both lab- and pilot-scale calciners are designed for low solids circulation rates, i.e. less than 30 kg m^{-2} s^{-1}, and with superficial gas velocities varying from 1.5 - 6 m s^{-1}. Assuming the density of the particles like the one from CaCO3, i.e. 1320 kg.m^{-3}, the calciners reviewed fall in the low-density CFB region based on the classification of Sun and Zhu [33]. Therefore, the calciner of this model will be designed for the low-density fast fluidization regime. In a fast fluidized bed, two regions are encountered: the dense zone, which corresponds to the lower part of the riser where there is almost a constant solids volumetric fraction in the order of 0.15 - 0.22, and the lean zone, which is the zone that follows where solids are entrained and the solids volumetric fraction decreases progressively (Figure 21) [10]. In the lean zone, the flow structure is described as a core-annulus flow pattern. Then the cross-section of the lean zone is further divided into two regions: a dilute core with bed particles transported upwards by the fluidizing gas, and a dense and smaller annulus region where clusters flow down over the reactor wall. The clusters after traveling a certain distance, dissolve and detach themselves from the wall to be re-entrained into the core region where they mix with fresh particles at the bed temperature.

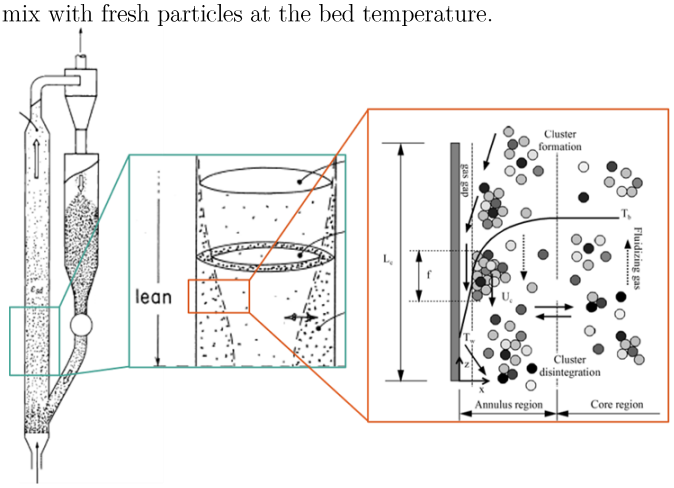

Fig. 4. Distribution of solids in the riser of a CFB. The image shows the core annulus regions with the cluster formation and the gas gap over the heat transfer surface. Modified from Kunii and Levenspiel [11] and Blaszczuk [12].

5.1. Proposed model assumptions

For the implementation of the proposed mathematical model several assumptions where taken:

a) In the balance equations, the diffusivity terms are neglected
b) The process in the reactor is a steady-state process
c) The static pressure inside the reactor due to the particles is neglected
d) The gas species can be assumed as ideal gases
e) Both in the dense zone and each dV of the lean zone the thermophysical properties of the flow species are constant
f) The volume fraction of the solids in the lean zone, as a function of z, is described by an adaptation of the Kunii and Levenspiel (K-L) model
g) The velocity of gas species is the same. The velocity of the solid species is the same.
h) The heat transfer in the lean zone will be described by a core-annulus model
i) The heat transfer between the reactor wall and the fluidized bed is modeled with a total heat transfer coefficient for each dV
j) The solid and the gas are in thermal equilibrium
k) The energy of the flow is due only to its enthalpy

5.2. Mass conservation analysis

The total mass balance for the solid and gas species are:

$$\frac{dm_{CaO}\ z}{dz} = M_{CaO} c_s\ z\ \ k_{calc}\ z\ (1 - X_{CaO}\ z\ )^{\frac{2}{3}}(c_{CO_2,eq} - c_{CO_2})A \tag{2}$$

$$\frac{dm_{CaCO_3}(z)}{dz} = -M_{CaCO_3} c_s(z) k_{calc}(z)(X_{CaCO_3}(z))^{\frac{2}{3}}(c_{CO_2,eq} - c_{CO_2})\ A \tag{3}$$

where m is the mass flow rate, M is the molar mass, c_s is the total number of moles of the solid components per unit of volume reactor, X is the molar fraction, c_{CO_2} is the local concentration of CO_2, and A is the cross-section area. The kinetic constant of $CaCO_3$ calcination k_{calc} and the equilibrium concentration of CO_2 $c_{CO_2,equil}$ are proposed by Martinez et al. [13] and Fang et al. [14]:

$$k_{calc}(z) = 2.05 \times 10^3\ e^{-\frac{1.12\times10^5}{R\,T_b}} \tag{4}$$

$$c_{CO_2,eq}(z) = \frac{1.462\times10^{11}}{T_b} e^{-\frac{1.913\times10^4}{T_b}} \tag{5}$$

where R is the ideal constant gas in J mol^{-1} K^{-1} and T_b is the temperature of the bed. The mass flow rate of CO_2 can be obtained by mass flow rate conservation:

$$m_{CO_2}\ z\ = m_{CO_2}\ 0\ + m_s\ 0\ - m_s\ z \tag{6}$$

$$m_{CO_2}(0) = \bar{X}_{CO_2}(0) m_g(0) \tag{7}$$

where $\bar{X}$ is the mass fraction. To solve equations (1) and (2) it is needed to find equations that describe the solids concentration, the molar fraction of CaO, and the local concentration of CO_2:

$$c_s\ z\ = \frac{1}{U_s\ z\ A}\left(\frac{m_{CaO}\ z}{M_{CaO}} + \frac{m_{CaCO_3}\ z}{M_{CaCO_3}}\right) \tag{8}$$

$$X_{CaO}\ z\ = \frac{\frac{m_{CaO}\ z}{M_{CaO}}}{\frac{m_{CaO}(z)}{M_{CaO}} + \frac{m_{CaCO_3}(z)}{M_{CaCO_3}}} \tag{9}$$

$$c_{CO_2}(z) = \frac{m_{CO_2}(z)}{M_{CO_2} U_g(z) A\ \varepsilon_g(z)} \tag{10}$$

where U_s and U_g are the velocity of the solids and the gas, ε_g is the gas volumetric fraction. Then, the solids and gas velocities can be found as:

$$U_s = \frac{m_s}{\rho_s \varepsilon_s A} = \frac{1}{\varepsilon_s(z) A}\left(\frac{m_{CaO}(z)}{\rho_{CaO}} + \frac{m_{CaCO_3}(z)}{\rho_{CaCO_3}}\right) \tag{11}$$

$$U_g = \frac{m_g}{\rho_g \varepsilon_g A \; \frac{1}{\varepsilon_g(z) A}\left(\frac{m_{CO_2}(z)}{\rho_{CO_2}(z)} + \frac{m_{N_2}(z)}{\rho_{N_2}(z)}\right)} \tag{12}$$

5.3. Hydrodynamic Model

The solid and gas volumetric fraction $\boldsymbol{\varepsilon_s}$ and $\boldsymbol{\varepsilon_g}$ are described by the K-L model from Kunii and Levenspiel [10]:

$$\varepsilon_{s,lean}\ z\ = \varepsilon_s^* + (\varepsilon_{s,dense} - \varepsilon_s^*) e^{-a\,(z - H_{dense})} \tag{13}$$

$$\varepsilon_{g,lean}(z) = 1 - \ \varepsilon_{s,lean}(z) \tag{14}$$

where the subindex ***lean*** and ***dense*** are used to denote the dense and lean zone in the riser, ε_s^* is the saturation carrying capacity, $\boldsymbol{a}$ is the decay factor and $\boldsymbol{H_{dense}}$ is the height of the dense bed. Fig. 5 shows a sketch of the profile described by equation (13). Parameter a describes the "S" shape of $\varepsilon_s(z)$ in the initial part of the lean zone, ε_s^* is the asymptotic limit of $\varepsilon_s(z)$, corresponding to the saturated carrying capacity of the gas, and H_{dense} is a constant to change from the height z to the height in the lean zone. Equation (13) is based on data obtained for cold columns without reactions and with constant solids and gas mass flow rates along z, therefore, its use in this model is arguable. For cold columns with constant mass flow rates, the velocities changes are only due to the changes of ε_s and ε_g.To a lower volumetric fraction corresponds a higher velocity in order to keep the mass flow rate constant, and *vice-versa*. The gas velocity starts at its maximum and the solids velocity starts at its minimum. They change monotonically and by construction, they meet at the pneumatic transport conditions. When the mass flow rate and temperature change with z, as in the case of this study, the velocity has to change accordingly. In this case, the temperature is increasing and the gas mass flow rate is also increasing due to the release of CO_2. Therefore, the K-L model must be adapted in a way that its basics physics is kept but taking into consideration these new factors.

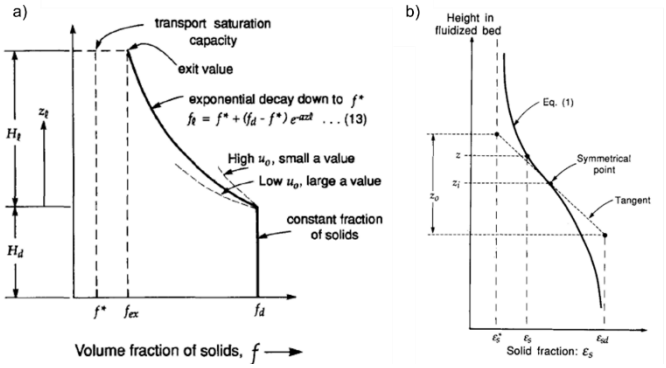

Fig. 5. Sketch of the solids volumetric fraction where f and ε are equivalent. a) gives an insight into the variables needed for K-L model [11] and b) shows the fitted distribution by Li and Kwauk [10]. The decay factor links both correlations and can be computed as $a = \frac{2}{z_0}$.

5.3.1. Solids volumetric fraction in the dense bed

The solids volumetric fraction in the dense zone is computed from a correlation obtained from a graph published by Kunii and Levenspiel [10]. The limits of the superficial gas velocity for the analyzed experimental data are between 1.5 to 5 m s^{-1}. Therefore, a constant value for higher velocities is defined in equation (15). The authors conclude that the superficial gas velocity seems not to affect appreciably the fractions of solids in the lower dense region.

$$\varepsilon_{s,dense} = \begin{cases} 0.2369\ U_0\ 0\ ^{-0.274} & U_0 \in [1.5\ ;5.0]\ \ \mathrm{m.s^{-1}} \\ 0.15 & U_0 > 5.0\ \mathrm{m.s^{-1}} \end{cases} \tag{15}$$

5.3.2. Saturation carrying capacity of the gas

The increase of temperature and mass flow rate of the gas will increase the gas velocity for the saturated carrying capacity condition. For this condition, the velocity of the solids is assumed to be the same as the velocity of the gas, i.e. pneumatic transport. A higher velocity of the solids corresponds to a smaller ε_s^*. This means that the ε_s^* for the reactor studied in this work is smaller than the one expected from the K-L model.

The differences in mass flow rates and densities create a mismatch between the conditions that characterize the "S" curve of $\varepsilon_s(z)$ at the beginning of the lean zone ($a = \frac{2}{z_0}$ where $\boldsymbol{z_0}$ is depicted in Fig. 5.b), and the conditions for the saturated carrying capacity. The $\varepsilon_s(z)$ profile, as predicted by K-L model may not capture the new physics and an impossible solution, with $U_s > U_g$, may occur, even though at the asymptotic limit $U_s^* = U_g^*$ is verified.

The constant a is not a local parameter, it is related to the shape of the "S" curve of $\varepsilon_s(z)$. Using lower values of a avoids $U_s > U_g$. However, the shape of the curve is defined in a short initial part of the lean zone. Forcing a low a seems not appropriate since the problem of the model arises from a low ε_s^*. Artificially increasing ε_s^* is the same as assuming that pneumatic transport will not occur. However, it is known from the literature that for these running conditions the pneumatic transport is a probable reality, even before the asymptotic limit. A better solution may be assuming a pneumatic transport as soon as $\varepsilon_s(z)$, as predicted by the K-L model, leads to $U_s = U_g$. During the pneumatic transport, the velocities will change while chemical reactions or temperature change occur, until $\varepsilon_{s\ z}\ = \varepsilon_s^*$. It is also important to have in mind that initial simulations and results reported in the literature show that the chemical reactions occur mainly in the first part of the reactor before this condition is verified.

The asymptotic value ε_s^* can be found for the asymptotic conditions, defined when solids and gas have the same velocity, and when complete calcination have been achieved. For a cold fluidized bed, this would be enough but for this case, something has to be assumed regarding the temperature of the bed. Thermal equilibrium with the wall could be a suitable choice. However, this will bring some doubts once the fixed wall temperature approach is abandoned to promote integration with the concentrating solar system. The suggested approach is to find if a wide range of expectable ε_s^* values have a small influence on the simulations results and, if it is so, choose a suitable ε_s^* to be used in the simulations. To find the expected range of ε_s^*, the temperature of the bed, in equilibrium with the wall, was tested within the interval $T^* \in [650\ ;\ 1000]$ °C using the following equations:

$$U_s^* = U_g^* \simeq U_0^* \tag{16}$$

$$\varepsilon_s^* = \frac{m_s^*}{\rho_s^* U_g^* A} \simeq \frac{m_s^*}{\rho_s^* U_0^* A} \tag{17}$$

$$m_s^* = m_{CaO}\ 0\ + \frac{M_{CaO}}{M_{CaCO_3}} m_{CaCO_3}\ 0 \tag{18}$$

$$\rho_s^* = \rho_{CaO} \tag{19}$$

$$U_0^* = \frac{m_g(0) + \frac{M_{CO_2}}{M_{CaCO_3}} m_{CaCO_3}(0)}{\rho_g^* A} \tag{20}$$

$$\rho_g^* = \frac{\rho_{CO_2}^* \rho_{N_2}^*}{(1 - \bar{X}_{CO_2}^*)\rho_{CO_2}^* + \bar{X}_{CO_2}^* \rho_{N_2}^*} \tag{21}$$

$$\bar{X}_{CO_2}^* = \frac{m_{CO_2}^*}{m_g^*} = \frac{m_{CO_2}(0) + \frac{M_{CO_2}}{M_{CaCO_3}} m_{CaCO_3}(0)}{m_g(0) + \frac{M_{CO_2}}{M_{CaCO_3}} m_{CaCO_3}(0)} \tag{22}$$

$$\rho_{N_2}^* = \frac{P}{R_{N_2} T^*} \quad ; \quad \rho_{CO_2}^* = \frac{P}{R_{CO_2} T^*} \tag{23}$$

5.3.3. Decay factor

The parameter a is presented in the literature as depending on a constant gas superficial velocity, which is not the case in this study. However, its value doesn't change too much in the lean zone,

therefore, an estimative will be made with a sensitivity study. For the estimative one could consider the value of U_0 at the midpoint of the lean zone. However, to find it an initial simulation has to be done. Another possible approach is to use the range of a that can be found in the experimental literature. Kunii and Levenspiel [10] present experimental results from Lu and Wang (1985) for running conditions similar to the ones in this study, although with constant mass flow rates. Based on those results, a lies in the interval $a \in \left[\frac{4}{U_0}; \frac{12}{U_0}\right]$ m^{-1} where $\boldsymbol{U_0}$ is the superficial gas velocity which is the velocity the gas would have if it occupied the whole section of the reactor:

$$U_g = \frac{m_g}{\rho_g \varepsilon_g A \ \frac{1}{\varepsilon_g(z) A}\left(\frac{m_{CO_2}(z)}{\rho_{CO_2}(z)} + \frac{m_{N_2}(z)}{\rho_{N_2}(z)}\right)} \tag{24}$$

5.3.4. Pneumatic transport condition

In the proposed adapted K-L model, after $U_s = U_g$ is achieved for the first time one has pneumatic transport. Then, ε_s is found from the equation:

$$\varepsilon_s\ z\ = \frac{\left(\frac{m_{CaO}\ z}{\rho_{CaO}} + \frac{m_{CaCO_3}\ z}{\rho_{CaCO_3}}\right)}{\left(\frac{m_{CaO}\ z}{\rho_{CaO}} + \frac{m_{CaCO_3}\ z}{\rho_{CaCO_3}}\right) + \left(\frac{m_{CO_2}\ z}{\rho_{CO_2}\ z} + \frac{m_{N_2}\ z}{\rho_{N_2}\ z}\right)} \tag{25}$$

5.4. Energy conservation analysis

The temperature of the bed can be solved as:

$$\frac{dT_b(z)}{dz} = \frac{1}{\sum_i m_i\ z\ C_{P_i}\ z}\left(H_{transf}\ z\ - H_{calc}\ z\ \right) \tag{26}$$

$$H_{calc}\ z\ =\ \Delta H_{calc} c_s\ z\ k_{calc}\ (1 - X_{CaO}\ z\ )^{\frac{2}{3}} \Delta \mathrm{c}_{CO_2} A \tag{27}$$

$$H_{transf}\ z\ = h_{w-b}\ z\ \ \pi\ D\ (T_w - T_b) \tag{28}$$

where the subscript $\boldsymbol{i}$ is the for solids and gas species.

From experimental campaigns in CFB risers, it is known that the walls of the riser are intermittently washed by clusters. Thus at a given time, one part of the wall is covered by clusters and the rest is in contact with a dilute gas-solid stream [55]. Different heat transfer mechanisms are involved: (1) convection/conduction from cluster to wall through a thin gas film, (2) radiation from clusters, (3) convection, and (4) radiation from the disperse phase. For practical reasons, an overall HTC is computed by summing up the individual heat transfer mechanism while taking into account the fraction of the wall that is in contact with the cluster δ_c while the rest is in contact with the dilute gas-solid stream. The overall HTC between the surface and the fluidized bed is:

$$\begin{aligned} h_{w-b}\ z\ = & \delta_c\ z\ \left(h_c\ z\ + h_{c,rad}\ z\ \right) + \\ & + (1 - \delta_c(z))(h_{d,con}(z) + h_{d,rad}(z)) \end{aligned} \tag{29}$$

where the subindices $\boldsymbol{c}$, $\boldsymbol{d}$, $\boldsymbol{con}$, and $\boldsymbol{rad}$ are to denote the cluster phase, dispersed phase, convection, and radiation respectively. The time-averaged fraction of the wall area covered by the clusters may be estimated as:

$$\delta_c(z)\ =\ 0.5\left(\frac{1 - \varepsilon_{cw}(z) - 0.00001}{1 - \varepsilon_c(z)}\right)^{0.5} \tag{30}$$

$$\varepsilon_{cw}(z)\ =\ \varepsilon_g^{3.811} \tag{31}$$

where ε_c is the gas volumetric fraction within the clusters, and ε_{cw} is the gas volumetric fraction near the wall.

5.4.1. Heat transfer coefficient from the dispersed phase

The wall is in contact with the upflowing disperse phase in the space between two clusters. The heat transfer coefficient from a dilute uniform suspension of a gas-solid mixture is used as an approximation as in Basu [15]:

$$h_d(z)\ =\ \frac{k_g\ C_{P_s}(z)}{d_p\ C_{P_g}(z)}\left(\frac{\rho_{dis}(z)}{\rho_s(z)}\right)^{0.3}\left(\frac{U_t^2}{g\ d_p}\right)^{0.21} Pr(z) \tag{32}$$

$$C_{P,s}(z) = \frac{m_{CaCO_3}(z)\ C_{P,CaCO_3}(z) + m_{CaO}(z)\ C_{P,CaO}(z)}{m_{CaCO_3}(z) + \ m_{CaO}(z)} \tag{33}$$

$$C_{pg}(z) = \frac{m_{CO_2}\ z\ \ C_{P,CO_2}(z) + m_{N_2}\ C_{P,N_2}(z)}{m_{CO_2}(z) + \ m_{N_2}} \tag{34}$$

where d_p is the particle diameter, $\boldsymbol{k}$ is the thermal conductivity, C_{P} is the specific heat, $\boldsymbol{U_t}$ is the terminal velocity of particles, and $\boldsymbol{g}$ is the gravitational acceleration constant. The density of the dispersed phase ρ_{dis} and the Prandtl number Pr are calculated as follows:

$$\rho_{dis}\ z\ =\ 1 - Y\ \ \rho_g\ z\ + Y\ \rho_s\ z \tag{35}$$

$$Pr\ \ z\ =\ C_{P,g}\ z\ \ \ \frac{\mu_g\ z}{k_q\ \ z} \tag{36}$$

where $\boldsymbol{Y}$ is the solid volumetric fraction of the disperse phase in the vicinity of the wall. Basu [15] found that a value of $\boldsymbol{Y} = 0.001$ % correlated well with experimental data, nevertheless, the author found that the HTC is insensitive to $\boldsymbol{Y}$.

The heat transfer coefficient of the radiation from the dispersed phase to the wall $h_{dis,rad}$ is computed based on the effective emissivity of a particle cloud considering scattering. Then the bed emissivity e_{dis} is calculated as in Brewster [16]:

$$h_{dis,rad}\ z\ = \frac{\sigma\ (T_b^4\ z\ - T_w^4)}{(\frac{1}{e_{dis}} + \frac{1}{e_w} - 1)(T_b\ z\ - T_w\ z\ )} \tag{37}$$

$$e_{dis} = \left[\frac{e_s}{0.5\ \ 1 - \ e_s}\left(2 + \frac{e_s}{0.5\ \ 1 - e_s}\right)\right]^{0.5} - \frac{e_s}{0.5\ 1 - e_s} \tag{38}$$

where e_w and e_s are the emissivity of the wall and the particle surface respectively.

5.4.2. Heat transfer from the cluster

The clusters are assumed to travel a certain distance, move away from the wall, disintegrate, and reform periodically in the riser [17]. While the cluster is in contact with the wall, it initially has the temperature of the bed. After that, a transient heat transfer between the wall and the cluster occurs. Initially, the first layer of clusters at the wall is involved and their temperature approaches the temperature of the wall due to conduction. Particles of subsequent layers will also participate in this process if enough time is given [15]. The heat transfer from the cluster involves both the contact resistance on the wall and the conduction resistance of the cluster. The contact resistance corresponds to the thermal resistance offered by a gas film of a thickness that is a fraction of the particle diameter [15]. Then, the heat transfer coefficient from the cluster to the wall is:

$$h_c\ z\ = \frac{1}{\left(\frac{\pi\ t_c}{4 k_c\ z\ \ \rho_c\ z\ \ C_{P_c}\ z}\right)^{0.5} + \frac{d_p}{10\ K_{gf}\ z}} \tag{39}$$

where t_c is the average residence time of clusters on the wall, and K_{gf} is the thermal conductivity of gas in W m^{-1} K^{-1} evaluated at the mean gas-film temperature $T_{filmavg}$:

$$T_{filmavg}\ z\ \ = \frac{T_b\ z\ \ + \ T_w}{2} \tag{40}$$

$$\begin{aligned} K_{gf}\ z\ \ = & \ 10^{-3}(1.5207 \times 10^{-11}\ T_{filmavg}^3\ z\ - 4.8574 \times 10^{-8}\ T_{filmavg}^2\ z\ + \\ & + 1.0184 \times 10^{-4}\ T_{filmavg}\ z\ - 0.00039333) \end{aligned} \tag{41}$$

The remaining variables needed for the computation of equation (39) are found as follows:

$$k_c\ z\ = k_g\left(1 + \frac{\left(1 - \varepsilon_{g,c}\ z\ \right)\left(1 - \frac{k_g}{k_s}\right)}{\frac{k_g}{k_s} + 0.28\ \varepsilon_c^{\ 0.63\left(\frac{k_g}{k_s}\right)^{0.18}}}\right) + 0.1\ \rho_g\ z\ \ C_{P_g}\ z\ \ d_p\ U_{mf}\ z \tag{42}$$

$$\varepsilon_{g,c}\ z\ = 1 - 1.23\left(1 - \varepsilon_{\mathrm{g}}\ z\ \right)^{0.54} \tag{43}$$

$$C_{P_c}\ z\ = (1 - \varepsilon_c\ z\ )C_{P_s}\ z\ + \varepsilon_c\ C_{P_g}\ z \tag{44}$$

$$\rho_c\ z\ = (1 - \varepsilon_c\ z\ )\rho_s\ z\ + \varepsilon_c\ z\ \rho_g\ z \tag{45}$$

The heat transfer coefficient of the radiation from the clusters to the wall $h_{c,rad}$ is computed based on the emissivity of clusters considering multiple reflections of particles e_c and the temperature of the cluster T_c, as in Grace [18] and Basu [19] respectively:

$$h_{c,rad}\ z\ = \frac{\sigma\ (T_c^4\ z\ - T_w^4)}{(\frac{1}{e_c}+\frac{1}{e_w}-1)(T_c\ z\ - T_w)} \tag{46}$$

$$e_c = 0.5\ \ 1 + e_s \tag{47}$$

$$T_c\ z\ \ =\ T_w\ + 1.29\left(\frac{\rho_{susp}\ z}{\rho_s\ z}\right)^{0.13}\ (T_b\ z\ \ -\ T_w) \tag{48}$$

$$\rho_{susp}\ z\ = \varepsilon_s\ z\ \ \rho_s\ z\ + \varepsilon_g\ z\ \ \rho_g\ z \tag{49}$$

where ρ_{susp} is the average suspension density.

5.5. Molar calcination efficiency and residence time of solids

The molar calcination efficiency η_{calc} can be understood as the fraction of $CaCO_3$ calcined in the reactor and it is calculated as:

$$\eta_{calc} \equiv \frac{X_{CaCO_3}\ 0\ - X_{CaCO_3}\ H_t}{X_{CaCO_3}\ 0} \tag{50}$$

where H_t is the total height of the reactor. The efficiency of the reactor is correlated with the solids residence time. It is expected that the longer the residence time is, the higher the efficiency would be. Therefore, the residence time of solids can be found as:

$$\frac{dt(z)}{dz} = \frac{1}{U_s(z)} \tag{51}$$

6. Results

6.1. Parameters and conditions of the model

The input parameters and boundary conditions of the model are described in Table 3. The reactor diameter and height were selected based on the literature review of current CaL lab-scale available systems. The diameter for lab-scales ranges from 0.07 - 0.1 m for plants with thermal powers between 10 - 30 kW. Similarly, the reactor length for lab-scale calciners is in the range of 6 - 12 m. A value of 10 m height was selected as a reference for design purposes. The final height will be recommended based on the simulation results. The riser wall is assumed to be of stainless steel with a constant surface temperature of 900 °C. AISI 310S stainless steel was used as reference material to select the emissivity to be inputted in the model, i.e. 0.8 [20]. This type of steel was used for the absorber tube receiver on the experimental setup for an on-sun test on a unit at the 1 MW solar furnace of CNRS [21]. The operation of the reactor occurs at atmospheric pressures. The pressure chose for the reference case was 1.2×10^{-5} Pa. From experimental data, it was checked that static pressure inside the reactor due to the particles can be neglected [5]. A constant wall temperature of 900 °C is chosen. This value corresponds to the limit after which sintering of the particles increases. It is expected that the temperature of the bed reaches the temperature of the wall. The densities of the solids were obtained from laboratory measurement using a sample of sorbent with a particle diameter in the range of 250 - 350 µm. The $CaCO_3$ density measurement was done using a fresh sample. For the measurement of CaO density, a sample resulting from the calcination reaction (after one cycle) was used. The particle diameter selected for the reference case is 300 µm. A sensitivity study will be done over the particle range ($d_p\ \in$ [200 ; 400]) to assess its effect on the process efficiency.

6.1.1. Hydrodynamic parameters

The height of the dense bed was selected as 0.25 m for the reference case. This value was chosen after reviewing available experimental data from low-density CFB. After reviewing the work of Bidwe [5], Charitos et al. [4], Xu et al. [22], and Collado et al. [23], it is expected to have a very small bed of some tens of centimeters or even inexistent. This parameter will be evaluated in a sensitivity study by variating its value over the range of $H_d \in [0\ ;\ 1]$.

The decay factor is presented in the literature as depending on a constant superficial gas velocity. The reference value was selected based on the experimental results presented by Kunii and Levenspiel [10] where the superficial gas velocity will be calculated at the beginning of the lean zone. A sensitivity study will be performed in the range of the values proposed by the authors ($a \in \left[\frac{4}{U_0\ H_d}\ ;\ \frac{12}{U_0(H_d)}\right]$). The solids fraction at saturated carrying capacity condition were found in this study assuming that the particles are fully calcined and that they reach pneumatic transport conditions. For high-temperature reactions, as in this case, additional assumptions had to be added regarding the temperature of the bed. The suggested approach presented in section 5.3.2 allowed finding the expected range of ε_s^* for a temperature interval of 650 - 1000 °C. The obtained range was $\varepsilon_s^*\ \in [1.8 \times 10^{-4};\ 2.5 \times 10^{-4}\ ]$. It was also verified with this model that the results of the simulation are very insensitive to ε_s^*. The molar calcination efficiency obtained was $\eta \in [0.6802; 0.6810]$ for the interval limits. Therefore, a reference value of 2×10^{-4} will be used.

Table 3. Model input of the reactor and solid-gas flow parameters.

	Parameter	Value	Units
Reactor	D	0.1	m
	H	10	m
	e_w	0.8	-
	P	120000	Pa
	T_w	900	°C
Solid	d_p	300	µm
	ρ_{CaCO_3}	1320	kg.m^{-3}
	ρ_{CaO}	870	kg.m^{-3}
	M_{CaCO_3}	0.1	kg.mol^{-1}
	M_{CaO}	0.056	kg.mol^{-1}
	e_s	0.9	-
Gas	M_{CO_2}	0.044	kg.mol^{-1}
	M_{N_2}	0.1	kg.mol^{-1}
	R_{N_2}	296.8	J kg^{-1} K^{-1}
	R_{CO_2}	188.9	J kg^{-1} K^{-1}
Boundary Conditions	$m_s(0)$	0.02	m
	$m_g(0)$	0.02	m
	$x_{CaO}(0)$	0.05	kg.mol^{-1}
	$x_{CO2}(0)$	0.2	kg.mol^{-1}
	$T_b(0)$	650	°C
Hydrodynamics	a	$\frac{4}{U_0\ H_d}$	m
	H_d	0.25	m
	ε_s^*	2×10^{-4}	-

6.2. Inlet boundary conditions:

The solids circulation rate and the superficial gas velocity ranged from 0.6 - 5 kg m^{-2} s^{-1} and 2 - 6 m s^{-1} respectively in the reviewed calciners for CaL process [6], [24], [25]. This translates into solids and gas flow rates in the order of 0.02 kg s^{-1}. This value was selected as the reference value. The variation range for the sensitivity study is $m_g\ 0\ \in [0.015\ ;\ 0.025]$ and $m_s\ 0\ \in [0.005\ ;\ 0.025]$.

The inlet mass fractions of CaO and CO_2, $x_{CaO}\ 0$ and $x_{CO2}(0)$ respectively, were also selected according to experimental data. In the beginning, fresh $CaCO_3$ without any content of CaO is expected to be used. After the first cycle, the introduced mass flow of solids will correspond to the one recovered from the carbonator which will have a higher content of CaO due to the deactivation of the sorbent. Texeira et al. [26] concluded that the fraction of unreacted CaO is highly dependant on the type of sorbent used. It was found that for CaO precursors as dolomite, the fraction of unreacted CaO was much lower (i.e. 5 %) when compared with wastes of marble powder (i.e. 20 - 30 %). Therefore, a reference value for the inlet mass fraction of CaO of 5 % is selected. A sensitivity study will be conducted for a range of values of $x_{CaO}\ 0\ \in [0; 0.4]$. Similarly, the initial mass fraction of CO_2 selected for the reference case is 0.2.

From the literature, it is known that the local concentration of CO_2 highly affects the reaction rate. Therefore, a sensitivity study will be performed for the inlet mass fractions of CO_2 for typical values found in the literature ($x_{CO_2}\ 0\ \in [0\ ;0.35]$) [27].

The temperature of the bed at the inlet is assumed to be 650 °C as this is the temperature of the products at the outlet of the carbonator in CaL processes. However, for thermochemical energy storage in CSP systems, this temperature might drop depending on the conditions for storing the carbonation products. Thus, the need for preheating of the sorbent and the fluidizing gas will be also assessed in the sensitivity study ($T_b\ 0\ = [25\ ;\ 650]$).

6.3. *Model implementation with constant wall temperature*

With an increase in temperature, it is expected that the hydrodynamics in the riser differs from cold model test conditions (Fig. 6.a). Usually, authors use the hydrodynamic model proposed by Kunii and Levenspiel [10] for high-temperature reactive systems by assuming constant densities, constant superficial gas velocity, and constant mass flow rates [28],[29],[30]. Under these assumptions, for a lower volumetric fraction, a higher velocity is achieved to keep the mass flow rate constant, and vice-versa (Fig. 6.a). For a high-temperature system with variable mass flow rate, Fig. 6.b shows otherwise. A rise in temperature results and the CO_2 mass generation increases the superficial gas velocity because of the change of the gas density (green line in Fig. 6.b).

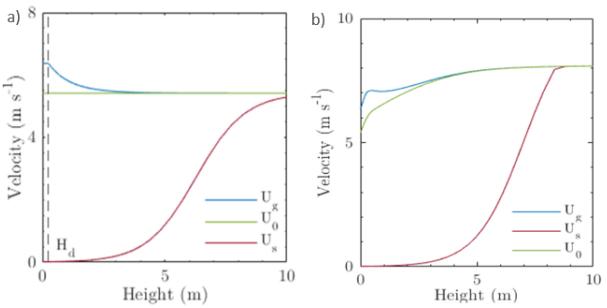

Fig. 6. Distribution of the solids and gas velocities along the axial direction of the calciner. a) Cold model case, b) Considers heat transfer and variable mass flow rate due to the reaction.

Fig. 7(a-c) shows the results related to heat transfer inside the reactor. The total heat transfer coefficient varies from 270 - 350 W m^{-2} K^{-1} and it is in the range of the reported values found in the literature [21], [15], [31]. In the dense bed, the fraction of cluster is set to zero and the HTC is computed as the contribution of the dense bed as a homogeneous dispersed phase. In the lean zone, the total HTC is computed as the sum of convective and radiative mechanisms from the disperse phase and clusters by taking into account the fraction of clusters at the wall. The cluster convection to the wall is in the order of 0.035 W m^{-2} K^{-1} and is negligible when compared to the other HT mechanisms. This agrees with the results from the example case presented in Basu [15]. Fig. 7.b shows that the heat flux from the wall to the bed steadily decreases until the reaction starts around 0.4 m. This height does not correspond to the height of the dense bed but to the point where the CO_2 equilibrium concentration surpasses the local CO_2 concentration as noticed in Fig. 8.a . The profile of the reaction rate in Fig. 8.b flattens around 7 meters, however, no significant contribution can be seen after 6 m height. Therefore, this gives some insight of the needed height of the reactor for the studied conditions.

The results obtained show that the bed temperature and the mass fraction of CO_2 at the inlet are the major factors affecting the conversion (Fig. 9) and therefore the molar calcination efficiency (Fig. 6.d). From the profiles, it is evident that the mass flow rate of the species remains constant until 0.4 m, i.e. the height at which the reaction starts. The molar fraction at 6 m and 10 m height for CaO is 0.68 and 0.72 respectively, and for CO_2 is 0.21 and 0.22. Similarly, the molar calcination efficiency at 6 m and 10 m heigh is 0.65 and 0.69. This justifies the selection of a reactor height of around 6 m for the operating conditions under study. It was proved that if constant densities and constant mass flow rates are assumed, as done by several authors in literature, this would lead to an overestimation of the molar calcination efficiency of 5 % points and 8 % points for 6 m and 10 m height respectively. The model presented in this work provides a more conservative result than when applying these simplifications

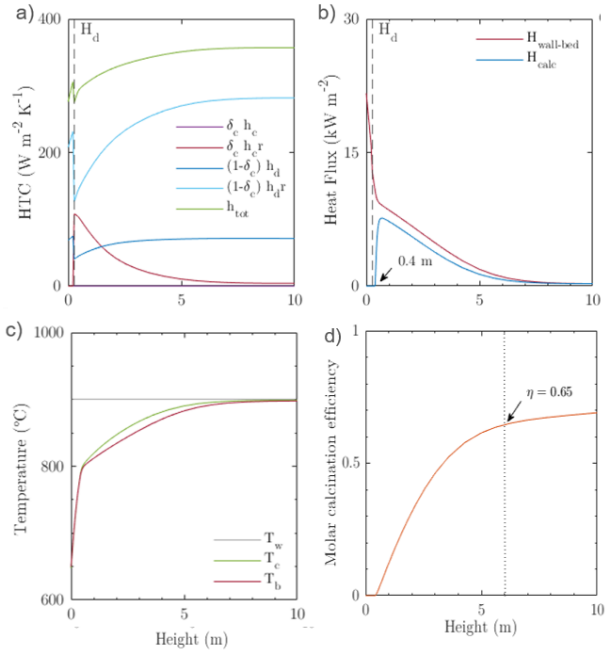

Fig. 7. Distribution along the axial direction of the calciner of a) total heat transfer coefficient, b) wall to bed heat flux, c) temperature profiles of the bed, wall, and clusters, and d) Molar calcination efficiency. A final efficiency of 0.69 is achieved at the end of the reactor height.

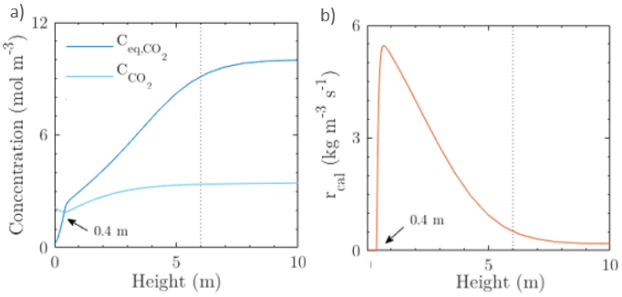

Fig. 8. Distribution along the axial direction of the calciner of a) CO_2 concentration in equilibrium and local CO_2 concentration and b) reaction rate.

6.3.1. *Sensitivity study*

To investigate the effect of several parameters in the calcination process, a sensitivity study was performed over the ranges described in section 6.1.

The decay factor was varied from 0.65 to 1.3: from the results, the molar calcination efficiency increases as the decay factor decrease (Fig. 10.a). The lower the decay factor is the longer the residence time of the particles is, hence the increased efficiency. The efficiency improves 47 % points when comparing results using the limit values of the variation interval. The decay factor affects greatly the velocity of solids. Therefore, it is necessary to confirm experimentally this parameter in a set up with high temperatures and variable mass flow rates.

The height of the dense bed was varied from 0 to 1 m: within this range, the efficiency improved 25 % points within the interval (Fig.

10.b). The increase of this parameter mainly displaces up the profiles of the solids volumetric fractions and the solids velocities leading to an increase of the residence time and the molar calcination efficiency for higher values of H_d. The effect of this parameter on the temperature of the bed is not that significant in the studied interval.

The particle diameter was varied from 200 to 400 μm: this parameter is used for the computation of heat transfer coefficients only. Results show that it does not have any significant effect on the temperature profile nor the molar calcination efficiency(Fig. 10.c).

The temperature of the bed was varied from 25 to 650 °C: Its variation showed to have major effects on the molar calcination efficiency achieved (Fig. 10.d). For ambient temperatures, the efficiency was the lowest of all the tests. The calcination reaction starts around 1.4 m. In this interval, the bed is heated up to 800 °C. After 800 °C the concentration of CO_2 in equilibrium surpasses the value of the local CO_2 concentration that is the driving force to start the reaction. As the inlet temperature rises, the process efficiency improves. An inlet temperature of 650 °C was selected as the favorable limit as this is the temperature the bed would have if it would have come directly from the carbonator. The improved efficiency is 27 % points. These results suggest the need of using a preheater for the gas and solids before being feed into the calciner and the use of a well-insulated storage system to decrease losses from daytime to night-time.

The initial mass fraction of CO_2 was varied from 0 to 35 %: For the lowest limit, i.e. 0 % of CO_2, the reaction starts at the very beginning of the reactor (Fig. 10.e). For the highest limit, the reaction starts around 0.7 m (Fig. 11) after the gas reaches 840 °C. At higher inlet CO_2 mass fractions, the initial local concentration of CO_2 is too high when compared to the one in equilibrium, therefore, the gas must be heated to a higher temperature for the reaction to start. The CO_2 mass fraction at the inlet is an important factor to be considered when designing the reactor for given conditions. These conditions should be established considering the carbonator.

The initial mass fraction of CaO was varied from 0 to 40 %: the calcination efficiency of 15 % point is obtained when comparing the limiting cases (Fig. 10.f). In the particular case of $X_{CaO}(0)$, the efficiencies obtained could be misleading when assessing the effect of the parameter. The molar calcination efficiency is defined as the ratio of the calcined sorbent to the inlet molar fraction of $CaCO_3$. The higher the content of CaO due to deactivation, the lower the content of $CaCO_3$ entering the calciner and the fewer sorbent available for calcination. This results in an improvement of the efficiency but only because less material is available to be calcined. Therefore, it could be beneficial to select enhanced sorbents to minimize their deactivation.

The gas and solids mass flow rate was varied from 0.005 to 0.25: the variation of these parameters resulted in improved efficiency of 36% points and 46 % point (Fig. 10.d). The case of m_g 0 $= 0.005$ shows a different pattern from the rest. This is a result of the ratio of gas and solids mass flow rate, which in this case is $\frac{m_g}{m_s} = \frac{0.005}{0.02} = 0.25$. At this condition, the achieved gas velocity is around 1.5 m s^{-1} which corresponds to conventional fluidized bed reactors where no entrainment is achieved. Therefore, this model is not valid to simulate this inlet condition but gives a hint about the fraction $m_g(0)/m_s(0)$ needed for achieving fast fluidization. Fig. 10.i shows the effect on the calcination efficiency measured at the end of the reactor when changing the ratio $m_g(0)/m_s(0)$. Even though the efficiency is measured at 10 m height, all the cases that achieve complete calcination in Figure 41 do it at shorter heights, i.e. 2 - 6 m. It can be concluded from this result that a ratio of at least 1.5 would be necessary to achieve complete calcination in a fast fluidization regime. In the reference case of this study, a ratio of 1 was being used. To increase the efficiency conserving the same ratio, it would be needed to decrease the mass flow rate of the gas and solid.

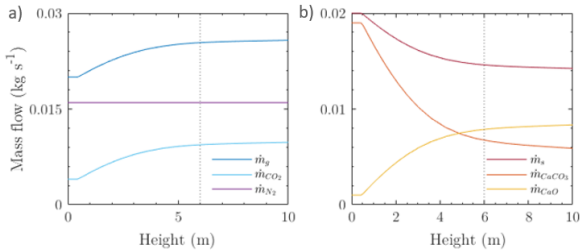

Fig. 9. Distribution along the axial direction of the calciner of a) mass flow rates of gas and b) solid phases species.

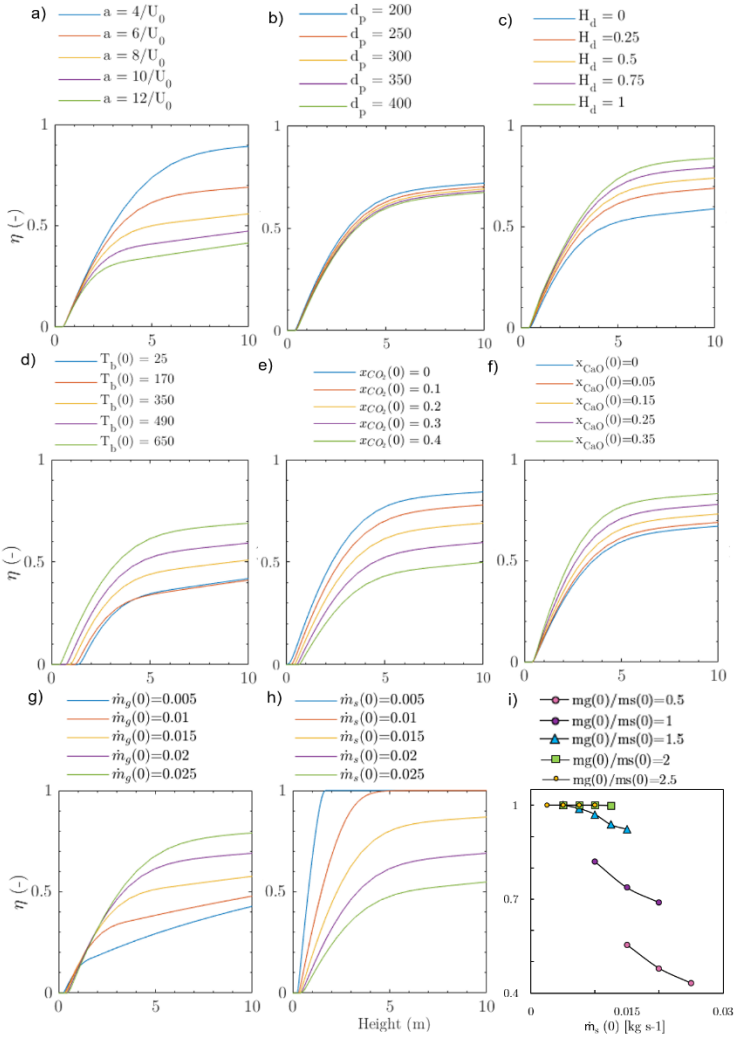

Fig. 10. Sensitivity study for a) decay factor, b) dense bed height, c) particle diameter, d) bed temperature, mass fraction of e) CO_2 and f) CaO, and mass flow rate of g) gas and h) solid.

6.4. *Model Implementation with Non-uniform Heat Flux*

The flux distributions on the receiver tube will strongly depend on the aiming point and control strategy of the solar field. Thus, a different flux distribution would result from a single aiming point strategy than from a multiple aiming point strategy. For this study case, a non-uniform flux in the vertical plane of the tube would be assumed as a starting point based on the results of Riaz and Gurr [32]. The flux is built as the sum of 2 gaussian distributions (Fig. 12.a in red), i.e. a multiple aiming point strategy. The total heat

transfer coefficient varies from 200 - 400 W m^{-2} K^{-1}. These values are in the range of the reported values found in the literature. Nevertheless, the range is much wider than in the case of the constant wall temperature. Fig. 12.a shows the calcination heat flux. The reaction starts at 1.3 m. As in the case with constant wall temperature, this height corresponds to the point where the CO_2 equilibrium concentration surpasses the local CO_2 concentration. After several tests varying the distribution of the heat flux used, the value of the efficiency fluctuated from 0.5 to 0.69. However, the temperature of the bed always reached 900 °C around 5 m height as shown in Fig. 12.b. This temperature marks the limit where sintering increases, therefore, it should be avoided. Future work is necessary to optimize the solar field by using an aiming strategy that allows to homogenize the flux distribution spatially and to avoid hotspots.

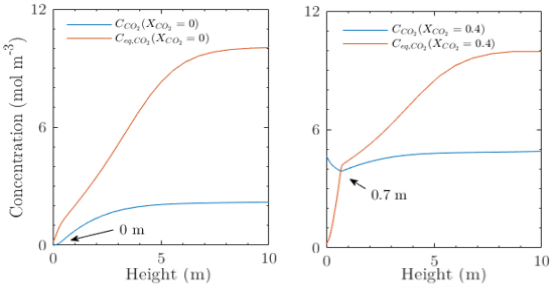

Fig. 11. Variation of the local concentration of CO_2 and its equilibrium concentration for the sensitivity study of the initial mass fraction of CO_2 in the fluidizing gas

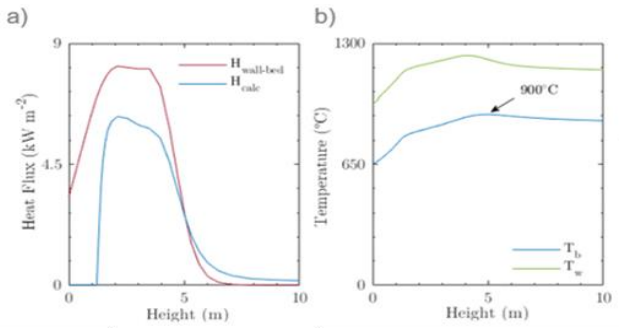

Fig. 12. Distribution along the axial direction of the calciner of a) wall-to-bed heat flux, b) temperature profiles of the bed and wall

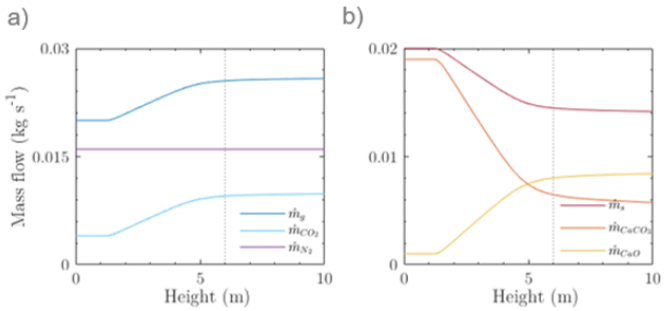

Fig. 13. Distribution along the axial direction of the calciner of a) mass flow rates of gas and b) solid phases species.

The achieved conversion is similar to the one for the case of constant wall temperature. Fig. 13 shows that the mass flow rates profile flattens after 6 m height. The molar calcination efficiency at 6 m and 10 m height is 0.66 and 0.7. Not much improvement is achieved after 6 m. However, this is a result of the imposed flux distribution which approaches zero around that height. After 6 m height, the calcination proceeds without flux at the expense of the internal energy of the bed (Fig. 12a). Improvements on using a more representative solar flux might variate the needed height.

6.4.1. *Sensitivity study*

In the sensitivity study of this case, the same parameters as in section 6.3.1 were evaluated. It was found that the only parameters with a strong effect on the molar calcination efficiency were the solids mass flow rate, the solid and gas mass flow rate ratio, and the temperature of the bed at the inlet. The reason for the negligible effect of the other parameters could be the distribution of the imposed heat flux, i.e. its peak is concentrated in the first half of the reactor while after 5 m it decreases dramatically to reach zero. From the results in section 6.3.1 it is known that the variation of the results is more significant in the second half of the reactor where the temperature of the bed approaches the temperature of the wall for a significant reactor length. Therefore, it was expected that in this case, where the temperature of the wall is not constant, the changes would be not as abrupt as in the previous case for the second half of the reactor. The temperature of the bed results stresses the importance of preheating the gas-solid flow (Fig. 14.a). For the flux distribution used, it was not possible to calcine the $CaCO_3$ sorbent with an initial temperature of the bed at ambient temperatures. The flux distribution used for the analysis is not enough to provide the power needed to heat the bed until a suitable temperature after which calcination can proceed. The effect of the temperature of the bed increased by 68 % points the molar calcination efficiency. Similarly, for the mass flow rate of solids the effect was significant, i.e. 47 % points of improved efficiency Fig. 14.a). When the ratio $m_g(0)/m_s(0)$ is changed in the analysis, the temperature of the bed and the wall rises as the mass flow rate of solids is lower. The temperature surpasses the limits imposed by sintering and the temperature that the wall material can stand.

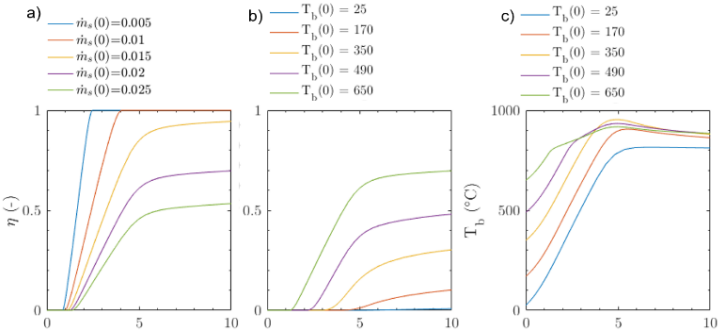

Fig. 14. Sensitivity study for a) mass flow rate of the gas, and b, c) the bed temperature of the bed at the inlet.

7. Conclusions

A unidimensional, steady-state computational model coupling heat transfer, hydrodynamics, and chemical reaction kinetics was presented for a calciner to be used as a solar reactor for Thermochemical Energy Storage (TCES) in Concentrating Solar Power (CSP) systems. The selected reactor consisted of an absorber tube enclosed within a reflective cylindrical cavity, where the absorber tube is also the riser of a Circulating Fluidized Bed (CFB) where the calcination reaction proceeds. The proposed model uses the calcination reaction kinetics proposed by Martinez et al. [13], the core-annulus heat transfer model, and a modified version of the K-L model of Kunii and Levenspiel [10]. The original K-L model is based on cold models, therefore, it was modified to account for the mass generation from the chemical reaction and the high temperature of the bed. With the proposed model, it was verified that assuming a constant temperature and constant mass flow rate, leads to an overestimation of the efficiency up to 8 % point. The model was implemented for two cases: (1) imposing a constant temperature of the reactor wall and (2) imposing a non-uniform flux distribution on the wall. In both cases, the bed temperature and the difference of the equilibrium concentration of CO_2 and its local concentration proved to be the main driving forces of the reaction. A fraction of the height of the reactor was

needed in both cases for heating the gas stream up to a point where the equilibrium concentration of CO_2 surpasses its local concentration. The needed height was 0.4 m and 1.3 m for cases 1 and 2 respectively. For a constant wall temperature, the needed height is much lower than in the case of the imposed flux. However, from experience, it is known that is highly unlikely to have a constant temperature on the receiver wall. Then, the control strategy of the solar field should be optimized to obtain a non-zero flux distribution on the base of the tube that allows decreasing the height of the reactor. This would result in some construction implications during the building of the receiver, e.g. adding a second concentrator at the reactor base. From case 1, it was concluded that the required height of the reactor under the reference operating conditions was around 6 meters height as no significant improvement in the efficiency was achieved at higher heights. A sensitivity study was performed to analyze the influence of the inlet conditions and some model parameters. It was found that the decay factor affects greatly the solids velocity resulting in a significant difference in the molar calcination efficiency. The variation of the height of the bed in an interval from 0 to 1 m did not show to be significant when compared to other parameters. Similarly, the effect of the particle size for the studied interval showed to be negligible. As for the sensitivity study of the inlet parameters, the inlet temperature of the bed, and the initial concentration of CO_2 were the ones with stronger effects on the molar calcination efficiency. An increase in the inlet concentration of CO_2 results in a higher temperature of the bed needed for the calcination reaction to proceed. Therefore, when the final design of the calcium looping with the storage system is designed, it is necessary to consider the concentration of CO_2 resulting from the carbonation process. For the inlet temperature of the bed, it was concluded that the preheating of the gas-solid flow is necessary to improve the process efficiency. Similarly, a well-insulated storage system should be designed to decrease thermal losses from daytime to night-time.

From the sensitivity analysis for the case where a non-uniform flux distribution is used, it was concluded that the results would be highly dependant on the aiming point and control strategy of the solar field. For the selected distribution, the temperature bed always reached the 900 °C which marks the limit where sintering of the sorbent increases. Therefore, it is necessary to optimize the solar field by using an aiming strategy that allows homogenizing the flux distribution spatially and to hotspots. The results show that after 6 m height there is not a greater improvement of the molar calcination efficiency, nevertheless, the small increase occurs at the expense of the internal energy of the bed. The effect of variating the decay factor, the gas mass flow rate, and the mass fraction of CO_2 at the inlet resulted to be less significant than in case 1. The results of the temperature of the bed again showed the importance of preheating the gas-solid flow. For the flux distribution used, the calcination reaction did not proceed when the temperature of the bed at the inlet was at ambient conditions. The results of this master thesis show that the developed model is a tool that allows distinguishing critical issues to be considered while designing the concept proposed in this work, CaL for TCES in CSP systems. Its simplicity and fast computation time allow the user to obtain quick results while testing how different parameters affect the performance of the reactor.

8. Acknowledgments

I would like to thank Prof. Filipe Medes, Eng. João Cardoso, Prof. Carla Pinhero, Prof. Henrique Matos, and Dr. Paula Texeira for your guidance, advice, and suggestions during this study.

9. References

[1] K. Lovegrove and W. Stein, *Concentrating solar power technology*. 2012.

[2] C. Ortiz, J. M. Valverde, R. Chacartegui, L. A. Perez-Maqueda, and P. Giménez, "The Calcium-Looping (CaCO3/CaO) process for thermochemical energy storage in Concentrating Solar Power plants," *Renewable and Sustainable Energy Reviews*, vol. 113. Pergamon, p. 109252, Oct. 2019, doi: 10.1016/j.rser.2019.109252.

[3] E. Alonso and M. Romero, "Review of experimental investigation on directly irradiated particles solar reactors," *Renewable and Sustainable Energy Reviews*, vol. 41. Pergamon, pp. 53–67, Jan. 2015, doi: 10.1016/j.rser.2014.08.027.

[4] A. Charitos *et al.*, "Experimental validation of the calcium looping CO2 capture process with two circulating fluidized bed carbonator reactors," *Ind. Eng. Chem. Res.*, vol. 50, no. 16, pp. 9685–9695, 2011, doi: 10.1021/ie200579f.

[5] A. R. Bidwe, "Hydrodynamic studies of the dual fluidized bed reactor systems for high temperature solid looping cycles," 2017.

[6] B. Arias, M. E. Diego, A. Méndez, M. Alonso, and J. C. Abanades, "Calcium looping performance under extreme oxy-fuel combustion conditions in the calciner," *Fuel*, vol. 222, no. January, pp. 711–717, 2018, doi: 10.1016/j.fuel.2018.02.163.

[7] M. Helbig, J. Hilz, M. Haaf, A. Daikeler, J. Ströhle, and B. Epple, "Long-term Carbonate Looping Testing in a 1 MWth Pilot Plant with Hard Coal and Lignite," *Energy Procedia*, vol. 114, no. November 2016, pp. 179–190, 2017, doi: 10.1016/j.egypro.2017.03.1160.

[8] J. Petrasch and J. Klausner, "Integrated solar thermochemical cycles for energy storage and fuelproduction," *WENE*, vol. 1, no. 3, pp. 347–361, Nov. 2012.

[9] G. Zsembinszki, A. Sole, C. Barreneche, C. Prieto, A. I. Fernández, and L. F. Cabeza, "Review of reactors with potential use in thermochemical energy storage in concentrated solar power plants," *Energies*, vol. 11, no. 9, p. 2358, Sep. 2018, doi: 10.3390/en11092358.

[10] Kunii and Levenspiel, *High-velocity fluidization*. 1991.

[11] D. Kunii and O. Levenspiel, "The K-L reactor model for circulating fluidized beds," *Chem. Eng. Sci.*, vol. 55, no. 20, pp. 4563–4570, 2000, doi: 10.1016/S0009-2509(00)00073-7.

[12] A. Błaszczuk, "Effect of flue gas recirculation on heat transfer in a supercritical circulating fluidized bed combustor," *Arch. Thermodyn.*, vol. 36, no. 3, pp. 61–83, 2015, doi: 10.1515/aoter-2015-0022.

[13] I. Martínez, G. Grasa, R. Murillo, B. Arias, and J. C. Abanades, "Modelling the continuous calcination of CaCO3 in a Ca-looping system," *Chem. Eng. J.*, vol. 215–216, pp. 174–181, 2013, doi: 10.1016/j.cej.2012.09.134.

[14] F. Fan, Z. S. Li, and N. S. Cai, "Experiment and modeling of CO2 capture from flue gses at high temperature in a fluidized bed reactor with ca-based sorbents," *Energy and Fuels*, vol. 23, no. 1, pp. 207–216, 2009, doi: 10.1021/ef800474n.

[15] P. Basu, *Circulating fluidized bed boilers abroad*, vol. 54, no. 6. 2007.

[16] M. Q. Brewster, "Effective Absorptivity and Emissivity of Particulate Media With Application to a Fluidized Bed," *J. Heat Transfer*, vol. 108, no. 3, pp. 710–713, Aug. 1986, doi: 10.1115/1.3247000.

[17] P. Rusheljuk, "Heat transfer in CFB," pp. 167–174, 2006, [Online]. Available: https://pdfs.semanticscholar.org/bec3/40e68122fa8f67b0e1eca842d908523aaa74.pdf.

[18] J. R. Grace, "HYDRODYNAMICS OF GAS FLUIDIZED BEDS," in *Fluidized Bed Boilers*, Elsevier, 1984, pp. 13–30.

[19] A. Dutta and P. Basu, "An improved cluster-renewal model for the estimation of heat transfer coefficients on the furnace walls of commercial circulating fluidized bed boilers," *J. Heat Transfer*, vol. 126, no. 6, pp. 1040–1043, 2004, doi: 10.1115/1.1833360.

[20] D. Level, E. Guillot, J. Sans, J. Ballestrin, and E. Guillot, "Comparisons of the spectral emissivity measurements at high temperatures of stainless steel AISI 310S," *SFERA II Proj. FP7-INFRA-312643*, no. February, p. 32, 2014.

[21] H. Zhang *et al.*, "Particle circulation loops in solar energy capture and storage: Gas-solid flow and heat transfer considerations," *Appl. Energy*, vol. 161, pp. 206–224, 2016, doi: 10.1016/j.apenergy.2015.10.005.

[22] J. Xu *et al.*, "Effects of superficial gas velocity and static bed height on gas-solid flow characteristics in a 60-meter-high transparent CFB riser," *Chem. Eng. J.*, vol. 334, no. September 2017, pp. 545–557, 2018, doi: 10.1016/j.cej.2017.09.131.

[23] F. J. Collado, "New one-dimensional hydrodynamics of circulating fluidized bed risers," *Granul. Matter*, vol. 18, no. 4, pp. 1–14, 2016, doi: 10.1007/s10035-016-0674-5.

[24] A. Martínez, P. Lisbona, Y. Lara, and L. M. Romeo, "Carbonate looping cycle for CO2 capture: Hydrodynamic of complex CFB systems," *Energy Procedia*, vol. 4, pp. 410–416, 2011, doi: 10.1016/j.egypro.2011.01.069.

[25] LUT, *Model Based Analysis of the Post- Combustion Calcium Looping Process for Carbon Dioxide Capture*. 2013.

[26] P. Teixeira, I. Mohamed, A. Fernandes, J. Silva, F. Ribeiro, and C. I. C. Pinheiro, "Enhancement of sintering resistance of CaO-based sorbents using industrial waste resources for Ca-looping in the cement industry," *Sep. Purif. Technol.*, vol. 235, no. October 2019, p. 116190, 2020, doi: 10.1016/j.seppur.2019.116190.

[27] J. R. Fernandez, S. Turrado, and J. C. Abanades, "Calcination kinetics of cement raw meals under various CO 2 concentrations," *J. Phys. Chem. C*, vol. 119, pp. 1623–1641, 2015, doi: 10.1039/c9re00361d.

[28] A. M. Cormos and A. Simon, "Dynamic Modeling and Validation of Post-combustion Calcium-looping Process," in *Computer Aided Chemical Engineering*, vol. 33, Elsevier B.V., 2014, pp. 1645–1650.

[29] A. Lasheras, J. Ströhle, A. Galloy, and B. Epple, "Carbonate looping process simulation using a 1D fluidized bed model for the carbonator," *Int. J. Greenh. Gas Control*, vol. 5, no. 4, pp. 686–693, 2011, doi: 10.1016/j.ijggc.2011.01.005.

[30] F. Sattari, M. Tahmasebpoor, J. M. Valverde, C. Ortiz, and M. Mohammadpourfard, "Modelling of a fluidized bed carbonator reactor for post-combustion CO2 capture considering bed hydrodynamics and sorbent characteristics," *Chem. Eng. J.*, vol. 406, no. August 2020, p. 126762, 2021, doi: 10.1016/j.cej.2020.126762.

[31] H. M. Abdelmotalib, M. A. M. Youssef, A. A. Hassan, S. B. Youn, and I. T. Im, "Heat transfer process in gas-solid fluidized bed combustors: A review," *International Journal of Heat and Mass Transfer*, vol. 89. Elsevier Ltd, pp. 567–575, Jun. 09, 2015, doi: 10.1016/j.ijheatmasstransfer.2015.05.085.

[32] M. Riaz and T. Gurr, "Solar flux density distributions on central tower receivers," *Sol. Energy*, vol. 19, no. 2, pp. 185–194, 1977, doi: 10.1016/0038-092X(77)90057-3.